

Radio Frequency Birefringence in South Polar Ice and Implications for Neutrino Reconstruction

I. Kravchenko

University of Nebraska, Department of Physics and Astronomy, Lincoln, NE, 68588-0111

D. Besson, A. Ramos, J. Remmers

University of Kansas, Dept. of Physics and Astronomy, Lawrence, KS, 66045-7582

Abstract

Using a bistatic radar echo sounding (RES) system developed for calibration of the RICE particle astrophysics experiment at the South Pole, we have studied radio frequency (RF) reflections off the bedrock. The total propagation time of \sim ns-duration, vertically (\hat{z}) broadcast radio signals, as a function of polarization orientation in the horizontal plane, provides a direct probe of the geometry-dependence of the ice permittivity to a depth of 2.8 km. We observe clear birefringent asymmetries along \hat{z} in the lowest half of the ice sheet, at a fractional level \sim 0.3%. This result is in contrast to expectations based on measurements at Dome Fuji, for which birefringence was observed in the upper 1.5 km of the ice sheet. This effect, combined with the increased radio frequency attenuation expected near the bedrock, renders the lower half thickness of South Polar ice less favorable than the upper half of the ice sheet in terms of its ultra-high energy neutrino detection potential.

Introduction

The response of ice as a function of polarization (“birefringence”) is characterized by differences in either wavespeed or absorption along linear (generally orthogonal) axes. Over a km-scale pathlength, in the absence of any preferred in-ice direction, one might expect any time propagation asymmetry at the single-crystal level to be macroscopically mitigated by the randomness of the corresponding single-crystal orientation. In such a case, over a total pathlength l consisting of N unit steps, each characterized by an asymmetry b , the average propagation time along each polarization axis should have a Gaussian distribution, centered at l/c , with width $b\sqrt{N}l/Nc$. The asymmetry distribution would therefore be a Gaussian of width $\sigma_b = b\sqrt{2N}l/Nc$, centered at zero. For 1% birefringence ($b = 0.01$), $l=1000$ m, and step sizes corresponding to typical grain sizes (10^{-3} m, or $N=10^6$), we expect $\sigma_b \lesssim 0.1$ ns. If, however, bulk flow of the ice sheet results in a preferred in-ice direction much longer than typical grain sizes, the propagation time asymmetry can be $\mathcal{O}(10)$ ns.

Impact on Particle Astrophysics

Efforts are underway to use the Antarctic ice sheet as an ultra-high energy neutrino target (DeYoung, T., 2010; Kravchenko, I. and others, 2006; Gorham, P.W., and others, 2009). Neutrino-ice collisions result in the production of charged particles which emanate from the interaction point with velocities approaching the speed-of-light *in vacuo*: $v \rightarrow c$. In a medium with index-of-refraction $n > 1$, detection of the resulting Cherenkov radiation in either the near-UV (TeV-scale neutrinos) or radio wavelength regime (PeV-scale neutrinos) by a suite of sensors can be used to reconstruct the kinematics of the initial neutrino, provided the absorption and refraction of the original electromagnetic signal due to the intervening ice can be reliably estimated. The RICE experiment (Kravchenko, I. and others, 2006) demonstrated the feasibility of the radio-detection approach over the last decade. The Askaryan Radio Array (ARA) Collaboration (ARA, 2010) seeks to substantially enlarge the current RICE footprint at South Pole by instrumenting an 80 km^2 area over the period 2010-2015. Ice birefringence could result in an initially ns-scale RF pulse being resolved into two components, with a time stagger comparable to the signal duration itself, requiring a trigger system with a correspondingly long signal integration time. Complete characterization of the ice permittivity, as a function of depth, and also polarization is therefore essential in obtaining a reliable estimate of the neutrino detection efficiency.

Birefringence Measurements

Prior Direct Experimental Work

Dielectric studies of ice have been ongoing for nearly a century (Ehringhaus, A., 1917), with radio frequency studies well over half a century old (Auty, R. and R. Cole, 1952). The study of ice birefringence is itself a discipline which is also several decades old (Hargreaves N.D., 1978). At visible wavelengths (590 nm), ice exhibits a birefringent asymmetry of $\sim 0.3\%$. Early RF studies focused on single-crystal measurements in the lab, with complementary samples of data collected *in situ*. Even prior to the advent of ns-scale signal capture, the field was already quite mature, with estimates of birefringent asymmetries of order 1% (Hargreaves N.D., 1977).

To explain the asymmetry observed in those early *in situ* data, the possible effects of geometrically distorted air bubbles and/or other sources of in-ice density contrast, internal layering, and the inherent single-crystal anisotropy, macroscopically manifest as a preferred axis of the crystal orientation fabric (COF), were all considered. The physical mechanism for COF alignment, however, was not fully explained – experimental data up to that point contradicted the hypothesis that internal strain due to ice flow is exclusively responsible for the observed birefringence.

Briefly, crystal orientation correlates with depth as follows (Riffenburgh, B., 2008): i) In deeper Antarctic ice, crystals align with the horizontal glide plane; near the surface, there is no preferred orientation, ii) complete COF alignment results in an order-of-magnitude faster bulk flow than randomly oriented COF. Note the interplay between ice flow and COF alignment - as shear increases, COF alignment increases, which, in turn, facilitates ice flow. The effect can be particularly dramatic at ice divides (Martaan, C. and others, 2008), given the large internal strains expected at those locales. The correlation between COF alignment and ice flow was verified by an analysis of airborne radar (60 MHz) data taken in the vicinity of Vostok Station, where the derived East Antarctic COF alignment was found to corroborate direct Vostok ice core data (Siegert, M.J. and R.Kwok, 2000). That study produced many results relevant to our investigation – most notably the conclusion that the variation of echo strength with increasing depth indicates scattering dominated by density, acidity, and COF effects, in the top, middle, and bottom third of the ice sheet at Vostok. To the extent that birefringence results from COF, we would therefore expect that non-zero birefringence would be most noticeable for deeper returns. Similarly, airborne-sounding data taken at Dronning Maud Land, some 3000 km West of Vostok, were also compared against ice-core data (Eisen and others, 2007). 150 MHz pulses of 60 ns and 600 ns duration revealed the presence of an horizontally extended (~ 5 km) plane, at a depth of 2025–2045 m, or approximately 800 m above the bed. That deep reflector was found to be inconsistent with acidity scattering, and more compatible with a discontinuity in the COF. Direct comparison of Vostok, or Dronning Maud data to South Pole, however, must properly take into account the variation in ice flow due to the different underlying stratigraphy and the fact that much of the ice sheet at Vostok lies in proximity to a nearly resistance-less lake.

Over a length scale of tens of kilometers, South Polar ice is observed to flow at the surface with a velocity of approximately 9–10 m/yr (Price, P.B. and others, 2002) in a direction which corresponds to about 153° in the coordinate system used for these measurements (corresponding to the 40 degree West Longitude line). The velocity profile, as a function of depth, has been determined by Price *et al.* (Price, P.B. and others, 2002), and is reproduced in Figure 1. To the extent that ice flow shear implies COF-alignment, and COF-alignment is singly responsible for birefringence, we would therefore expect very little birefringence to a depth of ~ 2 km, with increasing birefringence at greater depths, if the ice flow at present is the same as the ice flow through the history of the ice sheet formation.

There have been several more recent (Matsuoka, K. and others, 2003, 2004) *in situ* measurements of Antarctic ice (Doake, C., H. Corr, and A. Jenkins, 2002; Doake, C. and others, 2003) which have also been interpreted as evidence for COF-induced birefringence. In a study of internal layer reflections conducted at Dome Fuji (Fujita, S. and S. Mae, 1993), co-polarized (transmitter [Tx] and receiver [Rx] antenna polarizations parallel, projected onto the horizontal plane) and cross-polarized (Tx and Rx perpendicular) measurements were made over the full azimuth. Signals broadcast at a given frequency using three-element Yagis were detected after internal scattering from within the ice; both π and $\pi/2$ modulations of the received amplitude were observed. Under the assumption that the ordinary and extra-ordinary birefringent axes are orthogonal, the latter was interpreted as due to birefringent-induced interference effects in the time-domain.

In particular, as the transmitter-receiver systems were rotated in azimuth, signal drops were observed at angles $(2m + 1)\pi/4$ (with m an integer) relative to the presumed horizontal COF-alignment, which were attributed to destructive interference between the ordinary vs. extra-ordinary signals at the broadcast wavelength. Those data(Matsuoka, K. and others, 2003) imply $\sim \lambda/2$ variation over a depth of 1500 meters, which (given that $\lambda_{ice} \sim 3$ m for 179 MHz in-ice broadcasts) imply a birefringent asymmetry of order 0.1%. The authors note that their measured birefringence is somewhat weaker at 60 MHz, although an authoritative recent study of pure laboratory ice obtained an asymmetry $\delta_{e'}$ of $1.07 \pm 0.23\%$ (Matsuoka, T. and others, 1997) at both 1 MHz and 39 GHz.

In a comprehensive attempt to model the Dome Fuji data, and neglecting any possible tilting of the reflecting internal layers (which must occur coherently over an aeral scale of order the Fresnel zone to be significant), the dependence of radar scattering on density, COF, and acidity effects were assessed(Matsuoka, K. and others, 2004). In principle, the type of scattering can be elucidated on the basis of signal strength: COF and acidity-based layers typically reflect -30 – -60 dB of the incident power; density scattering, integrated through a vertical chord is typically a factor 10 larger (in power). To the extent that acidity scattering is a pure conductivity effect, we would expect it to vary as the inverse of frequency. To the extent that density and COF scattering is due to a variation of $n(\omega)$, we would expect such scattering to show much weaker frequency dependence, depending on the proximity of Debye resonances. In order to simplify the interpretation of data, the authors made the assumption that one scattering effect was dominant, and that although all types of scattering can result in large cross-polarized signals, only COF produces anisotropic scattering which also gave the observed azimuthal interference patterns.

In 2006, our group previously used time-domain bedrock reflections observed at a site near Taylor Dome(Besson, D.Z. and others, 2008) to estimate a birefringent asymmetry of 0.12%, projected onto the vertical \hat{z} -axis (perpendicular to the surface). A lack of conclusive ice flow data at Taylor Dome prevented a correlation with the local ice flow direction from being established. A follow-up study in 2008(Besson, D., R. Keast and R. Velasco, 2009) at the South Pole searched for, but found no detectable azimuthal variation in echo return times through the upper 1600 m of the ice sheet.

Table 1 summarizes some recent birefringence measurements.

Table 1: Summary of recent birefringence measurements.

Group	Locale	$\delta_{e'}$ Result	Comment
(Hargreaves N.D., 1977)	Greenland	0.024–0.031%	
(Doake, C., H. Corr, and A. Jenkins, 2002)	Brunt Ice Shelf	>0.14–0.47%	
(Doake, C. and others, 2003)	George VI Ice Shelf	>0.05–0.15%	
(Matsuoka, T. and others, 1997)	Lab Ice	$\sim 3.4\%$	1 MHz – 39 GHz
(Fujita, S., and others, 1996)	Lab Ice	$(3.7 \pm 0.6)\%$	9.7 GHz
(Woodruff, A.H. and C. Doake, 1979)	Bach Ice Shelf	0.52%	
(Fujita, S., and others, 2003)	Mizuho Station	measurable	
(Fujita, S. and others, 2006)	Mizuho	1.5%–3.5%	frequency-domain
(Besson, D.Z. and others, 2008)	Taylor Dome	0.12%	time-domain

Experimental Configuration

The Martin A. Pomerantz Observatory (MAPO) building, located at the South Pole, is used to house the signal generator and data acquisition system used for our measurements. Two 1.25-cm thick LMR-500 coaxial cables, each approximately 40 m long, were fed from within MAPO through a conduit at the bottom of the building and out onto the snow, and connect to the transmitter and receiver horn antennas (separated by 50 m, and on opposite sides of the MAPO building), respectively. Complete details of this measurement, including calibration of antennas, amplifiers, filters, cables, and verification of both the thermal noise floor, as well as the determination of the polarization dependence of the output signal, are provided in our 2008 study, probing the upper half of the ice sheet(Besson, D., R. Keast and R. Velasco, 2009). Our experimental

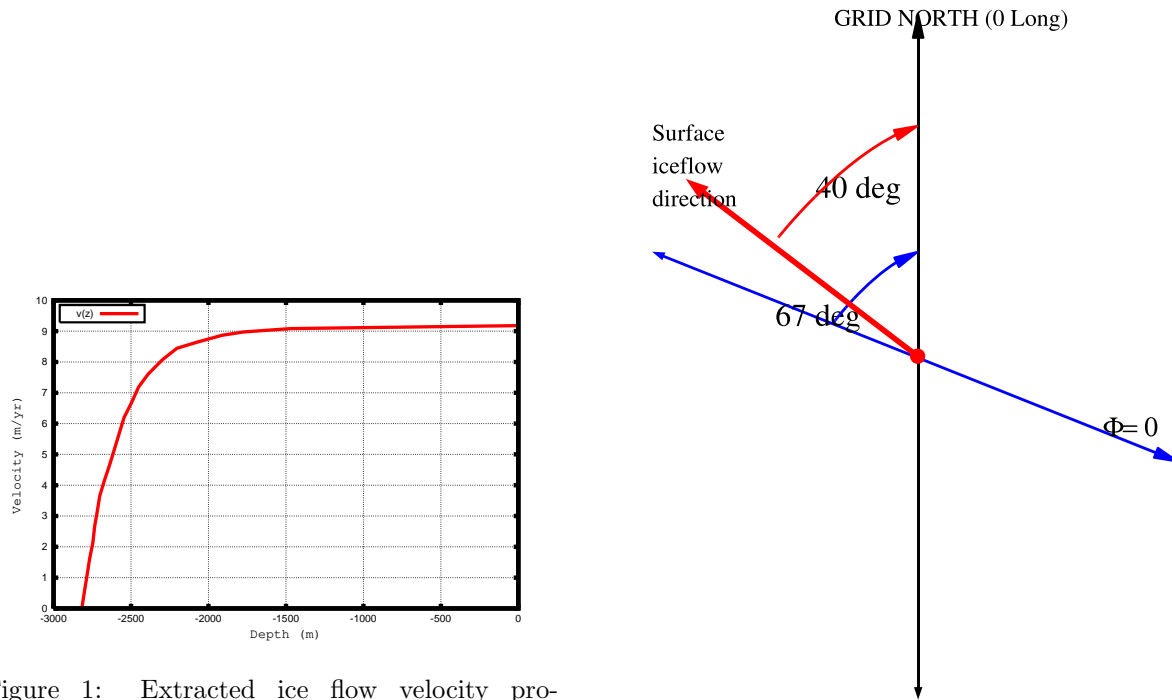


Figure 1: Extracted ice flow velocity profile vs. depth at South Pole, taken from (Price, P.B. and others, 2002).

Figure 2: Geometry of measurements presented herein. $\phi=0$ corresponds to the reference polarization orientation for TEM horns, chosen to correspond to the long axis of the MAPO building for convenience. Surface ice flow direction at South Pole is shown in red, corresponding to $\phi=-27^\circ$ ($\equiv+153^\circ$). Magnitude of surface ice flow is measured to be ~ 9 m/yr (Fig. 1), and uniform to a depth of ~ 2 km. (Data courtesy of Kurtis Skoog.)

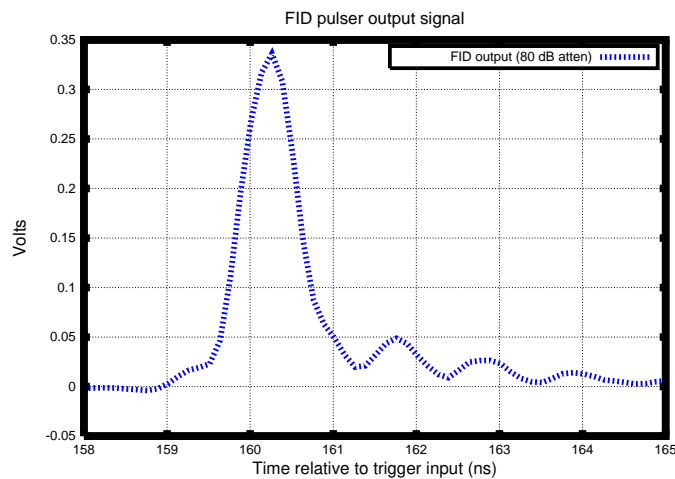


Figure 3: Output signal from FID pulser, attenuated by 80 dB.

geometry, relative to the surface ice flow axis, is identical to those previous measurements, and shown in Figure 2. As before, a LeCroy 950 Waverunner digital oscilloscope is used for data capture. The primary difference is that, for the measurements described herein, higher-power pulsers are used, with a maximum output voltage of ~ 3000 V. These higher-power pulsers now permit observation of the bottom reflection itself. To ensure consistent results, we employed two pulsers (Grant Corporation HYP5, and FID model FPG6-1PNK), two sets of antennas (a pair of TEM horn antennas built by the Institute of Nuclear Research [INR], Moscow, Russia and two Seavey Co. quad-ridge, dual-polarization antennas of the same type used by the ANITA experiment), and also two amplifier gains (36 dB, or 52 dB gain), with a variety of high-pass filters to allow multiple comparisons of signal shape and amplitude. The output signal shape from the FID pulser is shown in Figure 3. The combination of the FID pulser plus the INR horn antennas, at 36 dB gain, with 100 MHz high-pass filtering were found to yield the best signal-to-noise, without amplifier saturation. This configuration provides the bulk of the results herein, and is defined as the ‘Run 1’ configuration. To improve signal:noise, waveforms are typically averaged over ~ 10000 captures. Each averaged waveform is designated by the angle of the transmission polarization axis relative to our zero-degree reference (Fig. 2), as well as the corresponding angle for the receiver axis.

Observed Signals

We attempted to detect birefringent effects using the same approach as that used in our previous Taylor Dome analysis (Besson, D.Z. and others, 2008); namely, we search for a measurable time difference in received signals, as a function of the orientation of the long axis (transmitted signal polarization axis) of the horn antennas. Although the received spectral power is expected to be mostly determined by the λ^2 dependence of the horn antenna effective area, we have examined the signal strength as a function of frequency (transforming 32-ns [64-sample] time segments), as well, presuming that the frequency characteristics of the bedrock reflection may be differentiable from internal layer scattering, density scattering, etc. and thereby help elucidate distinct echoes.

The obtained voltages bracketing the time for the bedrock reflection ($\sim 34 \mu\text{s}$), as a function of rotation angle, are shown in Figure 4. As we sweep in azimuth, we note an apparent shift in the bedrock reflection time, between the zero degree and +30 degree orientation data sets. Figures 5 and 6 present the data for the -30 degree vs. +60 degree orientations, zooming in around the expected bedrock reflection time to illustrate the ~ 50 ns time shift, and also showing the Fourier transform (FT).

By comparison, the echo returns observed at earlier times are shown in Figure 7 and zoomed in Figure 8. Based on the time stagger in the bedrock reflection, and assuming that the time delay is linear with ice depth, we would expect to observe a corresponding 20 ns delay at an echo time of $\sim 14 \mu\text{s}$. No such obvious shift is observed, consistent with the results obtained in our previous study (see Fig. 9, taken from our 2008 South Polar data analysis). Our data therefore suggest that the birefringent asymmetry is primarily generated in the lower half of the ice sheet.

Ideally, we would have sufficient resolution to observe discrete scattering layers near the bed, and thereby map the magnitude of the birefringent delay as a function of depth. Although a visual inspection of the waveforms reveals the presence of enhancements in the received voltage at echo times of ~ 24 and ~ 26 microseconds, they are not sufficiently convincing to allow an extraction of a birefringent asymmetry. Previous RES measurements have, in fact, similarly observed a lack of evident echoes in deep ice for ~ 10 microseconds preceding the bedrock echo (the so-called ‘Echo-Free Zone’ (EFZ) (Robin, 1977; Fujita, 1999; Matsuoka, 2003)) The EFZ is illustrated by the distribution of recorded voltages, corrected for averaging and amplification, for echo times greater than 25 microseconds, as shown in Figure 10. The expected rms voltage, assuming a 220 K environment and comparable system noise, and using $V_{rms} = \sqrt{4k_B T B}$ with k_B Boltzmann’s constant and B the bandwidth of our receiver system (~ 1 GHz) is approximately 20 microVolts.

Bedrock Echo Signal Shape

Figures 5 and 6 display an apparently extended signal shape, including some enhanced power apparently preceding the primary bedrock reflection. This extended signal shape, persisting for ~ 200 – 300 ns, was similarly

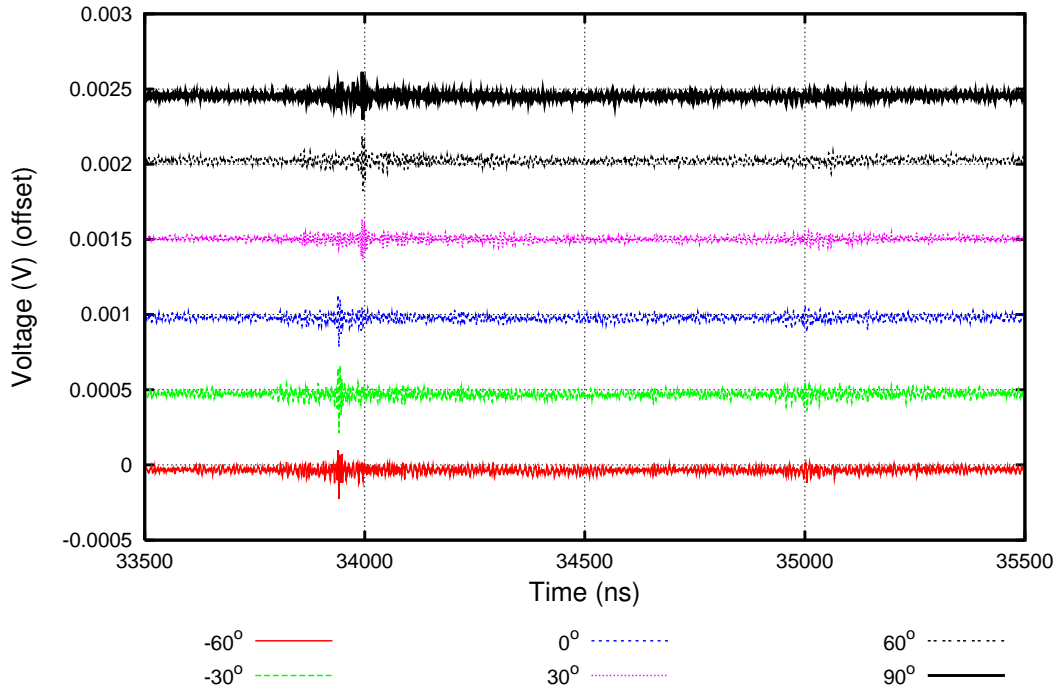


Figure 4: Measured voltages, as a function of co-polarization orientation of transmitter and receiver, for times consistent with the expected bedrock reflection. Waveforms have been vertically offset for clarity.

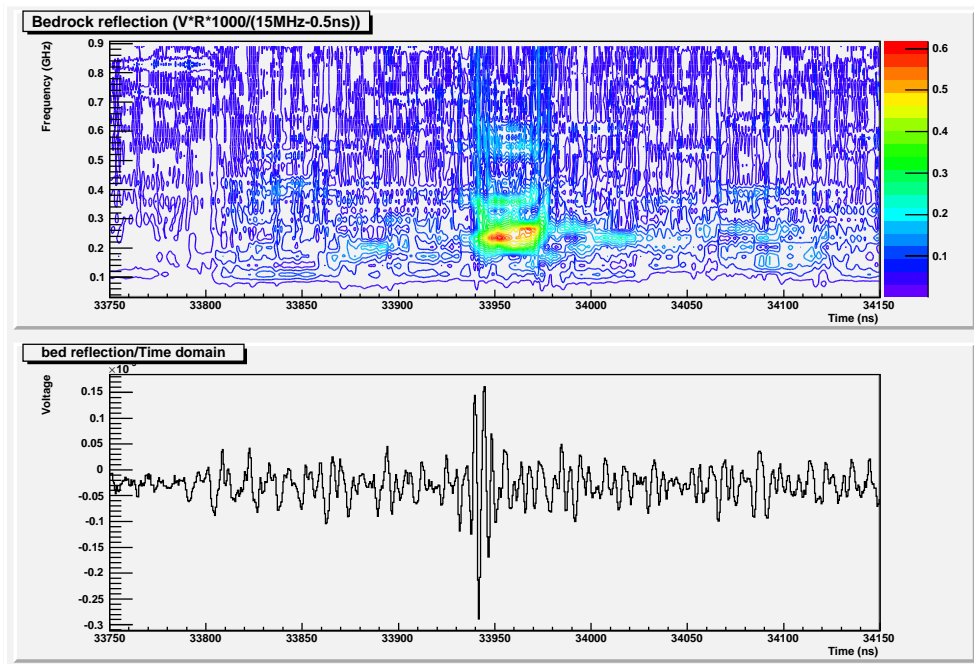


Figure 5: Power spectrum of received signal strength (relative units) for echo return consistent with time delay expected for bedrock reflection; antennas aligned at -30° .

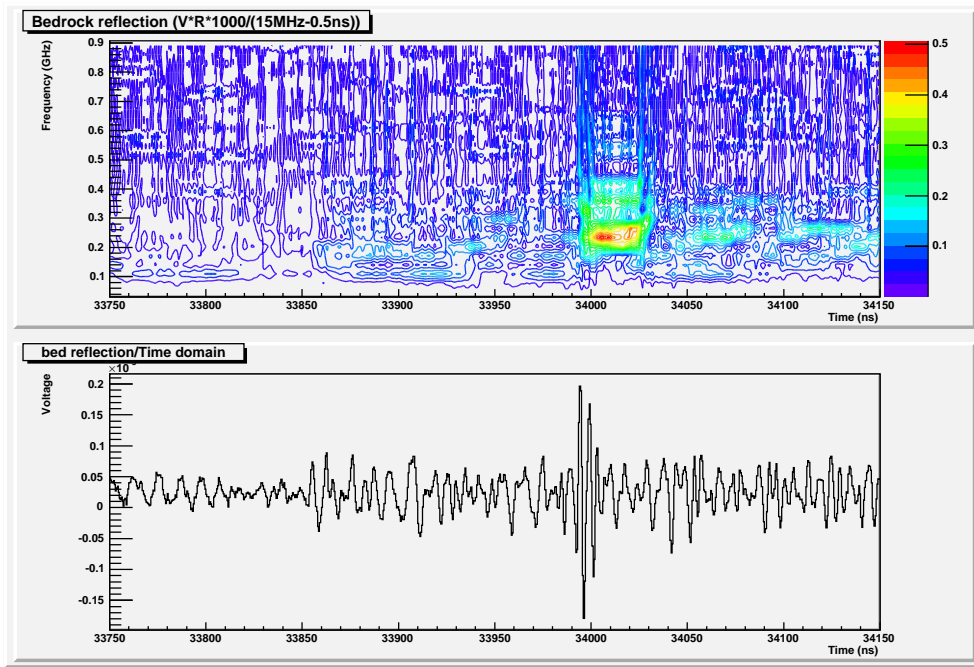


Figure 6: Power spectrum of received signal strength (relative units) for echo return consistent with time delay expected for bedrock reflection; antennas aligned at $+60^\circ$.

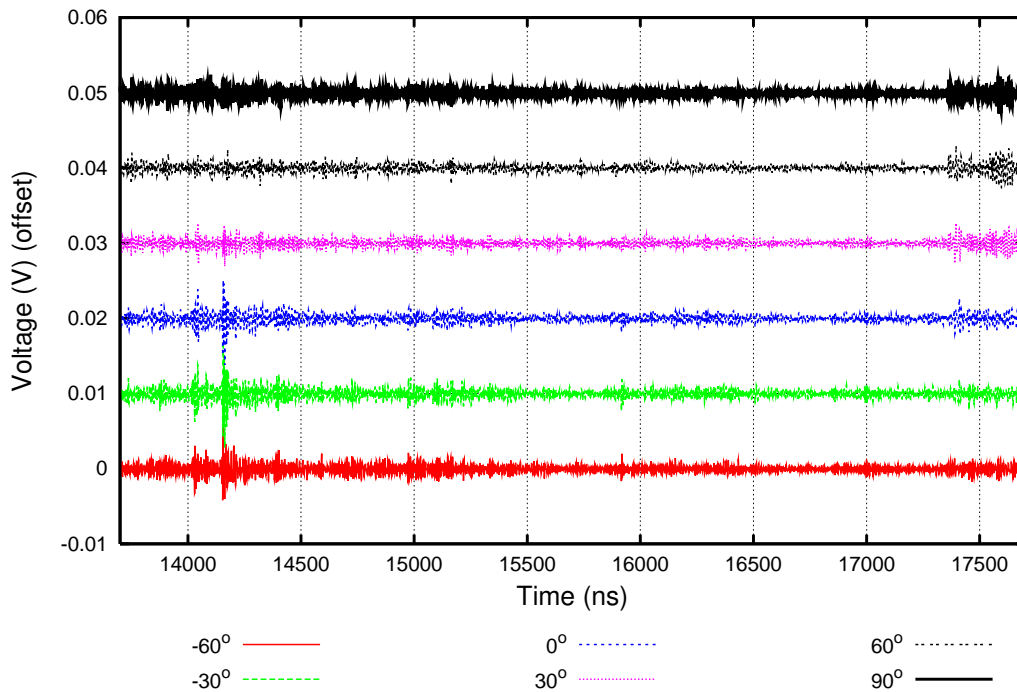


Figure 7: Measured voltages, as a function of co-polarization orientation of transmitter and receiver, for times consistent with reflections from within the ice itself. Upper five waveforms have been vertically offset for clarity.

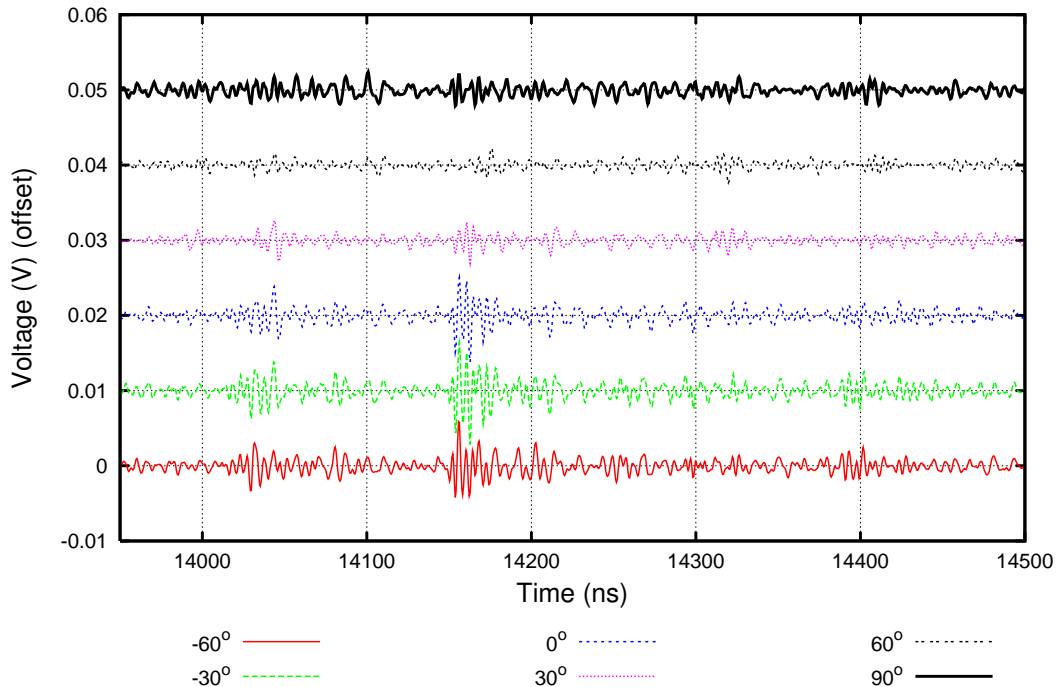


Figure 8: Zoom of previous figure.

observed in our studies at Taylor Dome, and is also present in the bedrock reflection data taken by ground-penetrating radar measurements from, e.g, the Center for Remote Sensing of Ice Sheets (CREGIS)(CREGIS, 2008). The primary reflecting area on the bedrock surface is expected to be roughly one Fresnel zone wide, or approximately $\sqrt{2\lambda d}$ in radius. With $\lambda \sim 1$ m, and $d \sim 5.6$ km, the time difference between a normally incident ray and a ray reflecting at the periphery of the first Fresnel zone should be $\sim (d/c)(1 + \lambda/d)$, or approximately 20 ns, considerably smaller than our observations. Given the typical antenna beamwidth of ~ 30 degrees in air (~ 20 degrees in ice), incoherent scattering extending across several Fresnel zones is therefore likely responsible for much of the signal extension observed. The assumption of incoherent scattering from macroscopic rubble near the bed is also consistent with our observation that signals observed with the Seavey antennas, which are responsive for frequencies greater than 250 MHz, are conspicuously more extended than the signals observed using the INR horns, which have good VSWR down to 100 MHz; longer-wavelength components should be less susceptible to decimeter-scaled bedrock scatterers. If the bottom 10 meters of the ice sheet also contains rubble, presumably resulting from glacial motion across the bed, the resulting scattering would also explain the apparent ‘pre-signal’ observed in several of the waveforms. The mixing of rock with basal water/ice was noted over 40 years ago after the first core to bedrock was extracted at Byrd Station(Gow, A.J. and others, 1968).

Consistency of observed birefringent asymmetry

Measurements were conducted using a variety of gains, as well as antennas. Due to varying locations of transmitter/receiver, as well as different instrumental delays, the absolute time of the measured bottom echo can shift. Nevertheless, for each separate ‘run’ (defined as one stable hardware configuration), when selecting the maximum voltage signal observed in the interval 33000–35000 ns return time, a time delay of approximately 53 ns was observed in the signal arrival times between the two modes (presumably corresponding to propagation along the major and minor birefringence axes), as we rotate antennas in azimuth, as illustrated in Figure 11.

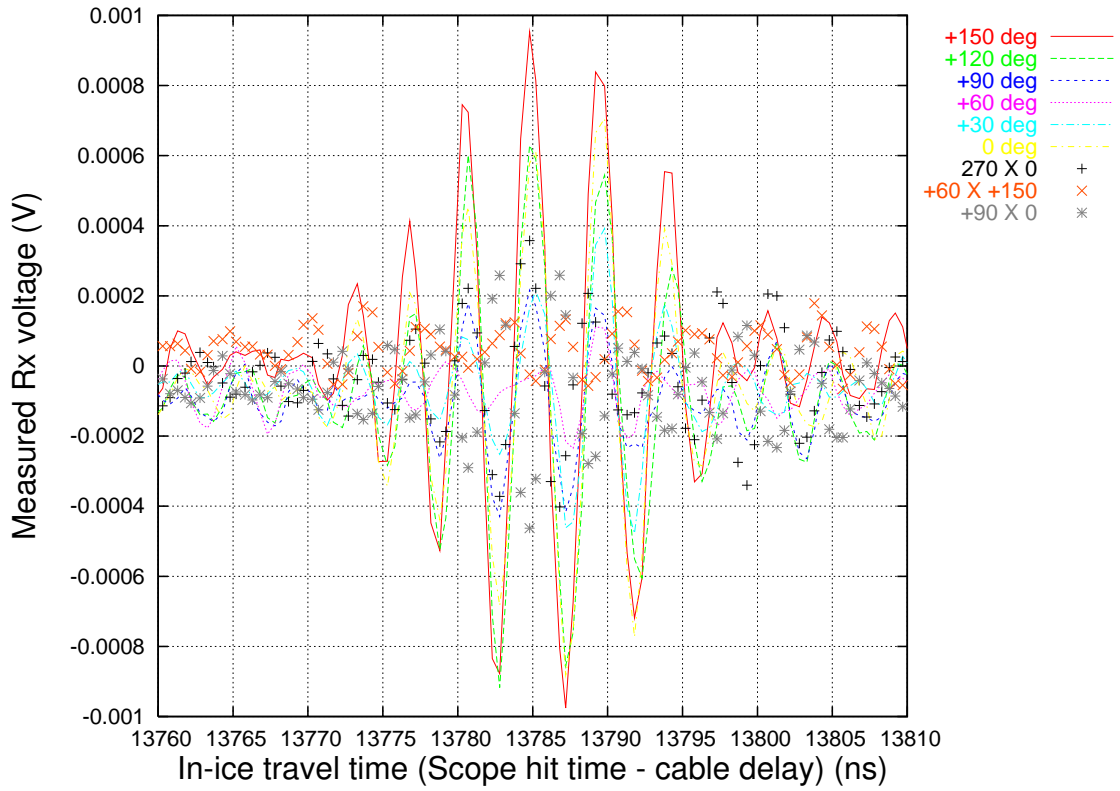


Figure 9: Ensemble of reflections observed in time interval around 14 microseconds after trigger, taken from 2008 South Polar data. Angular orientation convention is the same as for the current analysis. Cross-polarized reflections are shown as points in this plot.

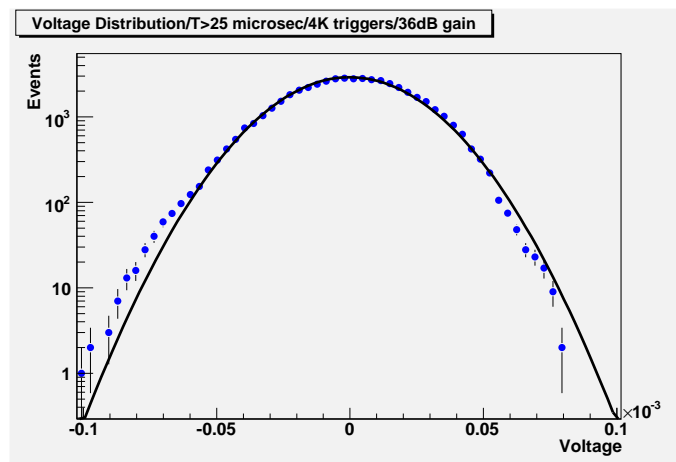


Figure 10: Gaussian fit to voltage distribution showing expected thermal-like characteristics.

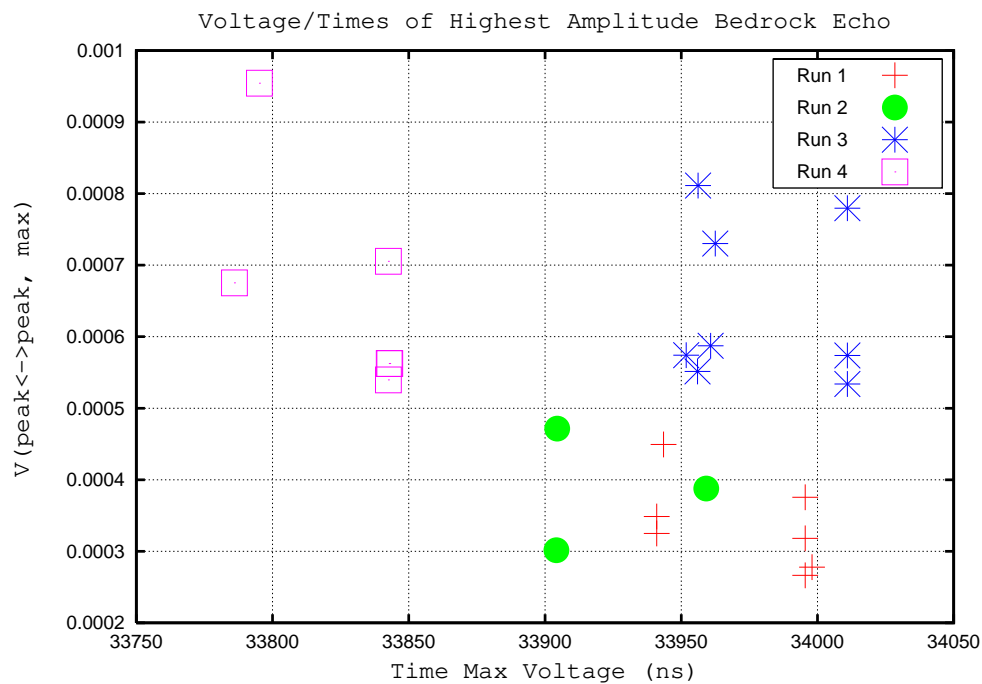


Figure 11: Time at which largest amplitude bedrock echo is registered in RICE data acquisition system. Runs are distinguished as follows: Run 1: FID pulser, 36 dB gain, two Moscow INR horn antennas used as Tx/Rx, 100-1000 MHz bandpass; Run 2: same as run 1, but with different cable lengths to antennas and antennas displaced on snow surface; Run 3: FID pulser, 52 dB gain (operating close to saturation), two Seavey antennas used as Tx/Rx, 250-1000 MHz bandpass; Run 4: HYPs pulser, 52 dB gain, Moscow INR horn antennas, 150-1000 MHz bandpass. Although the absolute echo times vary due to different run-to-run system delays, the time difference between the ‘early’ vs. ‘late’ times are consistently ≈ 50 ns.

Investigation of in-ice birefringence axis alignment

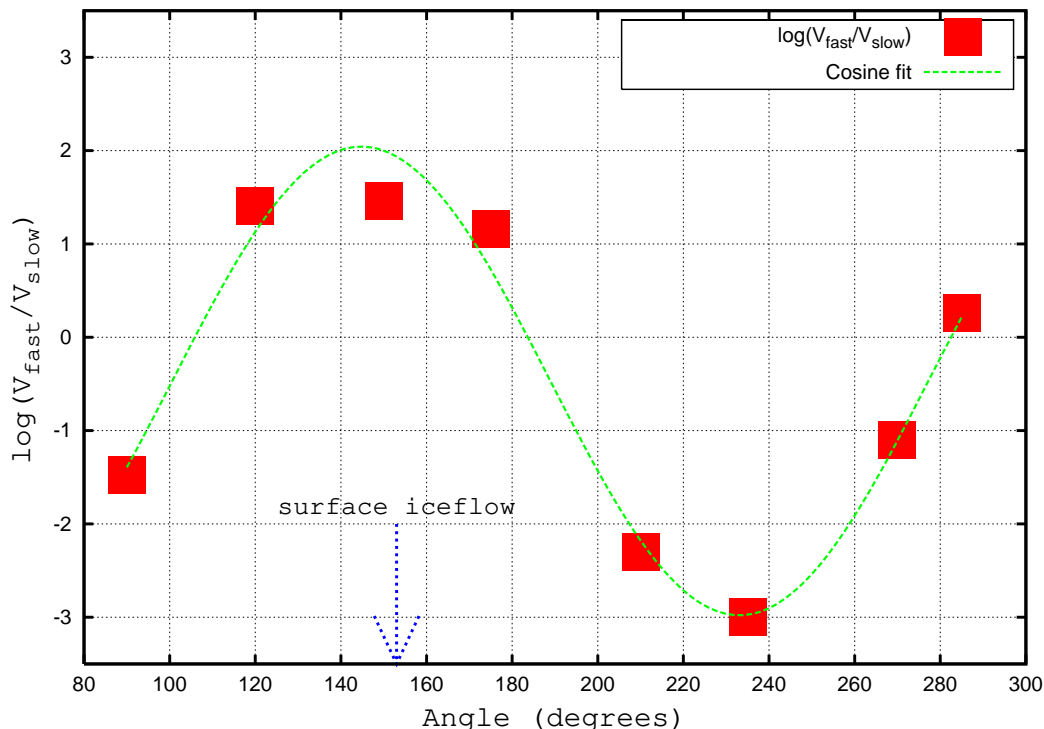


Figure 12: Ratio of peak-to-peak voltage measured for ‘early’ bedrock reflection (“V1”), relative to peak-to-peak voltage measured for ‘later’ bedrock reflection (“V2”), after subtraction of rms noise.

When broadcasting along one of the two birefringent axes, we expect to observe only one signal (assuming perfect isolation between the Vpol and Hpol terminals of our antennas); when broadcasting at 45 degrees relative to the two birefringent axes, we expect to observe equal amplitudes for the ‘early’ vs. ‘late’ received signals. We have summarized the relative amplitudes of the two signals in Figure 12; a value greater than 1 indicates that the ‘early’ signal was measured to have larger voltage (and vice versa). We note that this method of determining the optical axis orientation by the observed elliptical polarization is very similar to the formalism outlined over three decades ago by Hargreaves (Hargreaves N.D., 1977). Interpreted as due exclusively to birefringence, our data indicates that the birefringent axes are oriented at approximately -40 and 50 degrees, respectively, relative to the zero degree axis, or within 25 degrees of the local ice flow direction. Previous measurements of birefringence ((Doake, C., 1981; Woodruff, A.H. and C. Doake, 1979)) found a lack of clear correlation between the optical axis and the local ice flow direction; those prior measurements attributed the misalignment to a multi-step process leading to the in-ice crystal orientation. We cannot, of course, exclude the possibility that an asymmetry in the imaginary portion of the dielectric constant is responsible for at least some of the amplitude variation we are observing; Fujita *et al* (Fujita, S. and S. Mae, 1993) claimed an extreme difference of 15% in the loss tangent for broadcasts parallel vs. perpendicular to the optical axis.

Observed magnitudes of cross-polarized power

In the absence of birefringence, if we broadcast along one polarization, using antennas with excellent cross-polarization rejection, we would expect to observe little or no received signal in a receiver with perpendicular alignment. According to the manufacturer’s specifications for the Seavey antennas, the cross-polarization rejection between is approximately 10:1 in voltage (better than 20 dB rejection in power); we similarly measure better than 14 dB rejection in the lab for the INR antennas. Nevertheless, we note considerable cross-polarized power measured at our receivers, as shown in Figure 13. This is, in fact, not the first

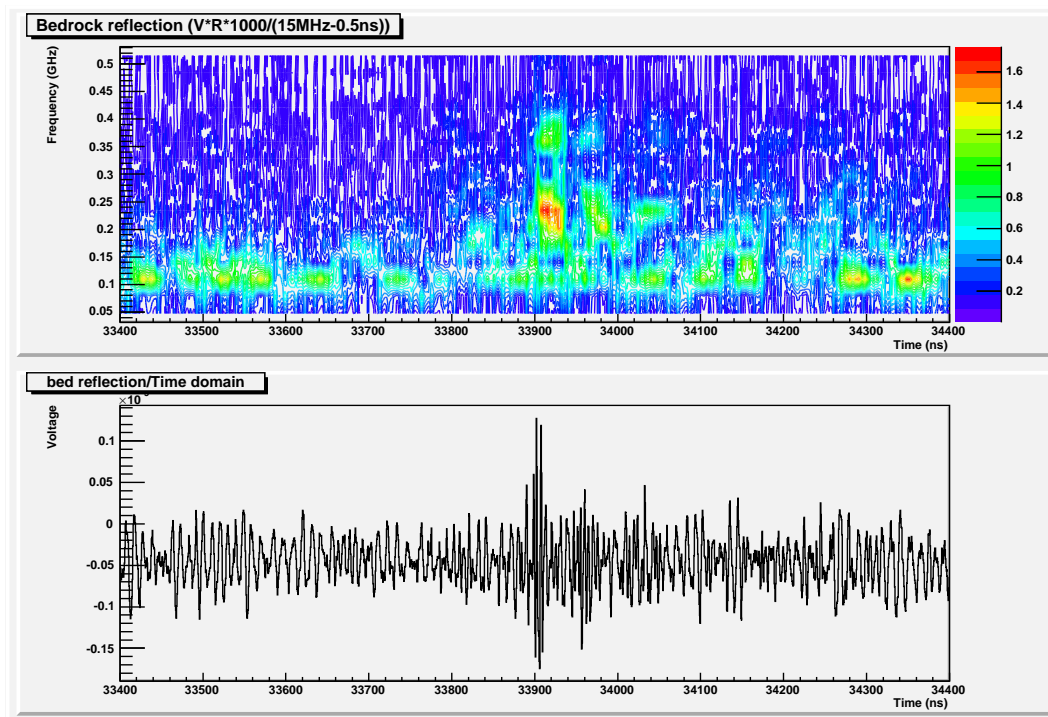


Figure 13: Run 1 data, illustrating received signal strength in cross-polarization orientation - transmitter at +90 degrees; receiver at 0 degrees.

observation of such co-polarization power at the Pole – a reported rotation of the basal echo by 90 degrees was reported over 40 years ago (Jiarcek, 1967), consistent with our 2004 bedrock reflection data from South Pole (Barwick, S., and others, 2005). For transmission at an angle θ relative to the ordinary axis, the signal amplitudes measured for the “fast” signal in the co-polarization vs. cross-polarization orientations should be $\cos^2 \theta$ and $\cos \theta \sin \theta$, respectively. Conversely, the signal amplitudes, projected onto the extraordinary axis, in the co-polarization vs. cross-polarization orientations should be $\sin^2 \theta$ and $\sin \theta \cos \theta$, respectively. If birefringence were solely responsible for the observed cross-polarized signal, we would therefore expect equal magnitudes of cross-polarized signal observed in all orientations, at variance with the observation in Figure 13. This suggests an additional mechanism is at least partly responsible for the amplitude variation observed for the early vs. late bedrock echoes.

Our 2008 analysis at South Pole (Besson, D., R. Keast and R. Velasco, 2009) also showed considerable observed cross-polarized signal strength for internal reflections, in a regime where the average birefringent effect was found to be consistent with zero; our measurements at Taylor Dome (Besson, D.Z. and others, 2008) displayed somewhat less cross-polarized power in the bedrock reflection, as shown in Figure 14. Echoes provided by polarization-grating-like reflectors, as well as the mechanism responsible for the observed extended bedrock echo signal shape may interfere with birefringent asymmetries. The fact that each of these has an associated, and generally unknown preferred axis complicates an unambiguous association of the amplitude data shown in Figure 12 with the birefringent asymmetry axis alone. If the reflecting plane is not horizontal, then there will also be an asymmetry generated upon reflection, for the electric field components perpendicular, and parallel to the reflecting surface, as well. In principle, Faraday rotation can also lead to considerable cross-polarized power;¹ however, a recent laboratory study of cold ice disfavors that possibility (Besson, D., R. Keast and R. Velasco, 2009).

¹Hargreaves excludes the possibility of detectable Faraday rotation, based on the premise that a forward rotation down to the base will be cancelled by a reverse rotation back to the surface. In fact, the phase inversion of the signal at the base results in non-cancellation.

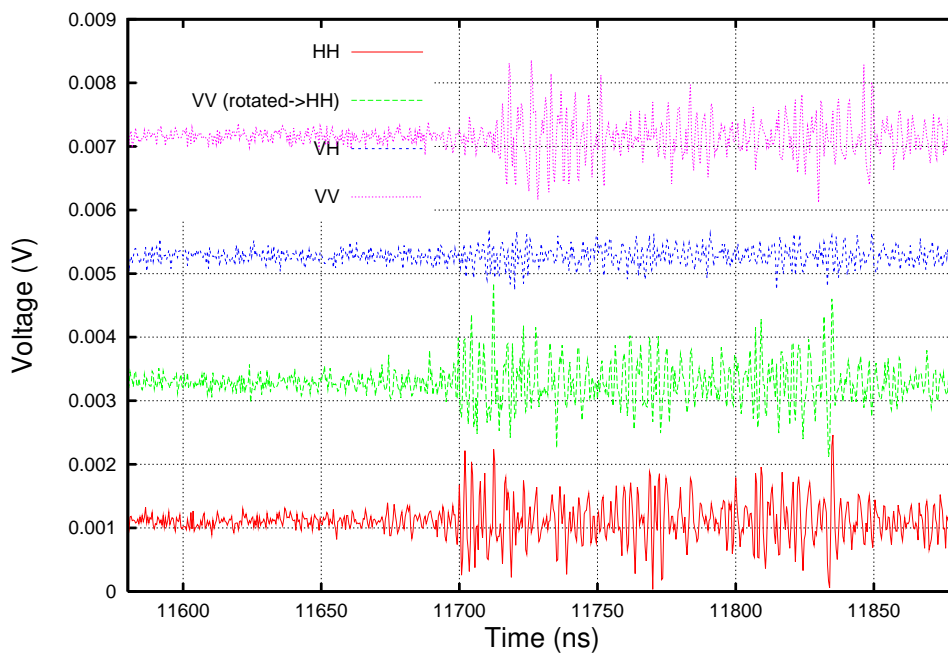


Figure 14: 2006 Taylor Dome data, showing received signal as a function of time for indicated orientations. “V” and “H” designate orthogonal Vertical and Horizontal terminals of Seavey antennas, respectively. “VV→HH rotate” refers to the Tx and Rx orientation for which the VV axes of both Tx and Rx have been rotated into the initial HH orientation. In this Figure, the three uppermost signals have been vertically offset to enhance visual clarity.

Estimate of bedrock depth

To determine the ice thickness at our measurement point, we use the average time delay observed for run 1 (33972 ns), corrected for the total cable delay (160.3 ns; Figure 3) and use a temperature-weighted average EM wave velocity of 169 ± 0.3 m/ μ s below the firn (Dowdeswell and Evans, 2004). Through the firn, we use direct measurements of radio propagation wavespeed (Kravchenko and others, 2005), implying a one-way transit time of 1102 ns through the upper 200 m of the ice sheet at South Pole. Taking the errors from (Dowdeswell and Evans, 2004) gives an implied depth of 2857 ± 5 m. However, field measurements of radio frequency wave velocity have shown variations in the permittivity of up to 1%; uncertainties in impurity levels can, in principle, contribute an approximately equivalent systematic error. Taken together, these imply a systematic depth error of ~ 30 m.

Amplitude Measurements - check of implied field attenuation length L_{atten}

Knowing the total cable length (~ 125 m), the cable loss per unit length (~ 5 dB/100 m at 500 MHz), the maximum signal amplitude at the output of the pulser (2.5 kV), the measured reflected signal amplitude V_{ice} , the bandpass of the antennas (~ 1 GHz), and the net gain of the amplifiers + filters in the system, we can determine “absolutely” the average attenuation length to the bed by direct application of the Friis Equation: $V_{Rx}/V_{Tx} = R\sqrt{G_{Tx}G_{Rx}}e^{-d_{tot}/L_{atten}}\lambda^2/(4\pi d_{tot})^2$, with R the bedrock reflectivity (taken to be 0.3), V_{Rx} and V_{Tx} the measured signal voltages, G the antenna gain of transmitter and receiver antenna (taken to be 12 dBi given the expected in-ice focusing, and consistent with values used for our previous 2004 analysis with the same antennas (Barwick, S., and others, 2005)), d_{tot} the total round-trip echo path (5.7 km), and λ the broadcast wavelength. Since we are using sharp time-domain signals, rather than the limited-duration ‘tone’s used for our previous, dedicated attenuation length study, we do not expect the same precision as attained in that previous study, and correspondingly use $\lambda=1$ meter as sufficient for this coarse check of the received signal amplitudes. Averaged over the entire vertical chord, we obtain an implied average attenuation length $L_{atten}=627$ m, entirely consistent with those 2004 measurements at Pole.

Comment on dispersion

By performing a Fourier transform on the received waveforms, we can investigate the dispersive characteristics of ice over the frequency range 200 MHz – 900 MHz. Figure 15 displays the Run 1 data at a Tx/Rx angle of -5 degrees. For this plot, the amplitude at high frequencies has been multiplied by frequency (squared) to compensate for the expected wavelength dependence of both receiver and transmitter effective height. From this Figure, we estimate synchronicity of received power to within 4 ns for all frequencies considered, implying a variation in the real part of the dielectric constant less than 0.012% over the range of frequencies considered in this analysis. This asymmetry is consistent with the naive expectation that the variation in dielectric constant with frequency should be relatively small at radio frequencies, far from Debye resonances for ice. By contrast, in their extensive review of radio ice sheet sounding, Dowdeswell and Evans (Dowdeswell and Evans, 2004) suggest a variation in the dielectric constant of approximately $\Delta\epsilon' \approx 0.04$ over the interval 1–100 MHz, corresponding to a wave speed variation of about 1.25%.

Implications for Neutrino Detection

An in-ice neutrino interaction can produce either a single particle (muon) propagating over km-scale distances, or a compact electromagnetic or hadronic shower, limited to ~ 10 m in extent. The former is best detected with suitably located photomultiplier tubes sensitive to UV radiation. The latter is best detected with englacial radio receivers sensitive to the expected \sim GHz bandwidth, 1-ns duration “Askaryan” signal impulse. Since the measured birefringent asymmetry is considerably larger in magnitude than 1 ns, a 1 GHz bandwidth receiver will generally observe ‘split’ signals, with relative amplitudes depending on the geometry and actual orientation of the optical axis relative to the signal propagation direction. Monte Carlo simulations indicate that, without compensating trigger electronics, the birefringent asymmetry measured here would result in an approximately 5% reduction in equivalent neutrino detection volume. The smallness of this effect is primarily due to the fact that a) the measured asymmetry is limited to deeper, poorer quality

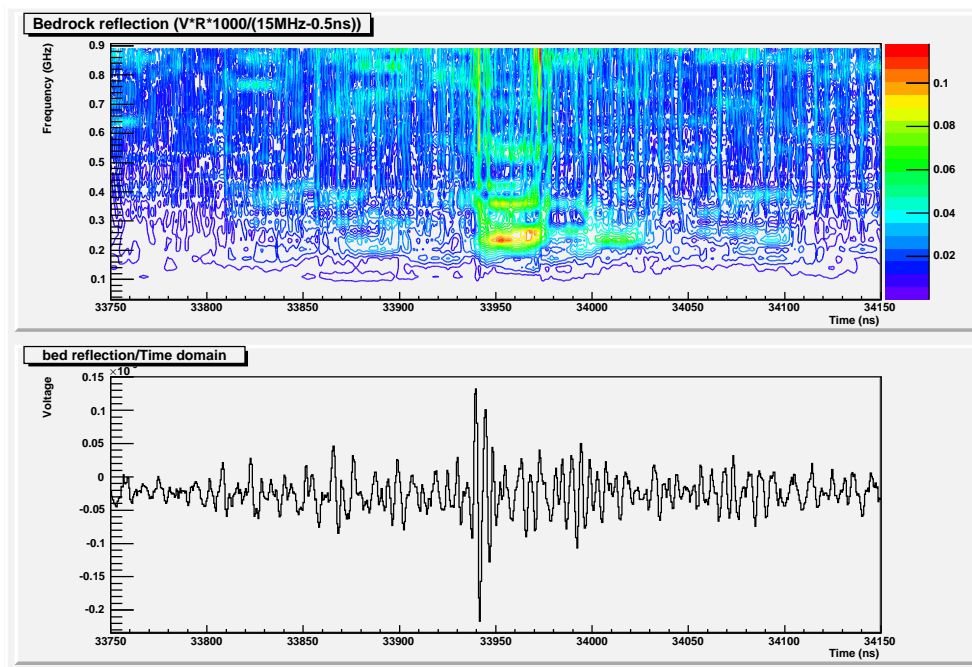


Figure 15: Time domain and frequency domain (top) bedrock echo observed for -5° orientation. We observe approximate synchronicity at all frequencies.

(from the standpoint of RF transmission) Polar ice, b) the measured asymmetry is restricted to the vertical axis, while neutrino signals are predominantly observed along near-horizontal incident angles.

Summary and plan for additional work

We have measured a birefringent effect, in the lower half of the ice sheet at South Pole. The magnitude of the observed effect ($\sim 0.3\%$) is approximately consistent with other measurements of the radio frequency properties of cold polar ice. It would be desirable to correlate our measurement with direct physical measurements of South Polar ice down to the bed. Unfortunately, despite having perhaps the most developed infrastructural base in the Antarctic interior, an ice core of the type taken at Siple Dome, Dome C, Monning Draud or Vostok has not yet been extracted. Such a core would provide incontrovertible, and direct evidence for the COF correlation only suggested by our current measurements. If such an association could be verified, the application of birefringent and/or COF measurements to perform glacial tomography could potentially develop as a discipline unto its own (Eisen and others, 2007, 2006). The fact that our measurements for the upper half of the ice sheet are in direct contradiction to those made at Dome Fuji imply that the ice characteristics are considerably different between those two locales; the fact that the interior is often regarded as one monolithic glacial mass notwithstanding. Our results are, however, in agreement with the analysis of data taken in the vicinity of Vostok, which found evidence for COF scattering dominating only in the lowest third of the ice sheet, in agreement with direct core data (Siegert, M.J. and R.Kwok, 2000).

A follow-up measurement would accumulate more cross-polarization data, with yet a higher-power pulser, and attempt to further elucidate the birefringent dependence on depth. As Hargreaves (Hargreaves N.D., 1977) points out, rotation of transmitter/receiver antennas through the full azimuth in the cross-polarization orientation vs. rotation of Tx/Rx in the co-polarization orientation allows one to separate out effects due to birefringence vs. effects due to asymmetric reflecting planes. Assuming different reflection coefficients in the x- vs. y-directions (R_x and R_y), the maximum signal measured with transmitter perpendicular to the receiver, compared to the minimum signal measured in the same configuration allows an extraction of R_x vs. R_y . The matrix-based approach of Fujita *et al.* (Fujita, S. and others, 2006) also allows a separation of the various contributions to anisotropic scattering based on a comprehensive analysis of the elliptical polar-

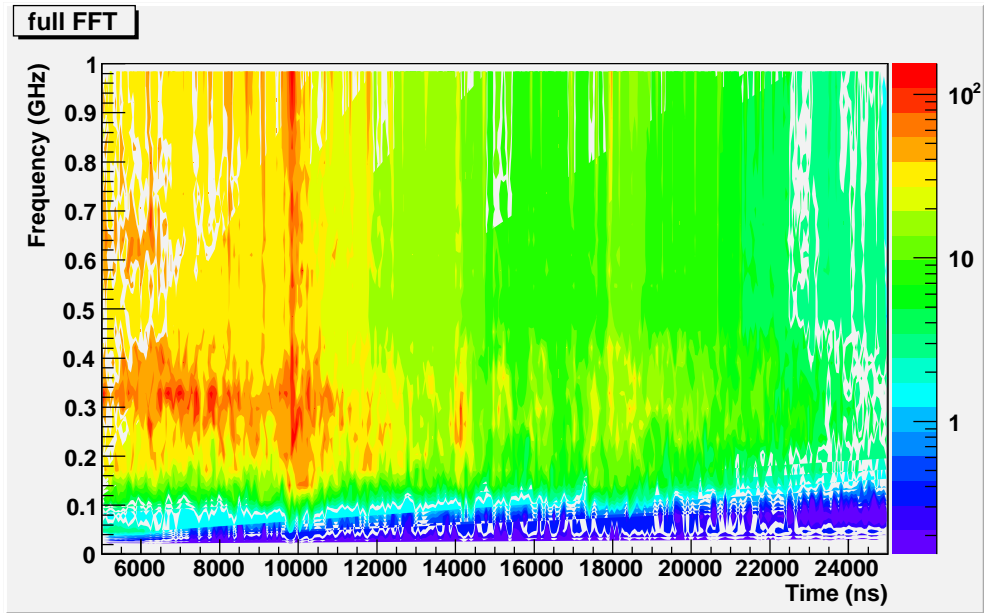


Figure 16: Frequency domain amplitude observed for 0° orientation, as a function of depth. Voltages have been scaled by $(frequency)^2$ to compensate for transmitter/receiver frequency response.

ization characteristics over a broad range of geometries and depths. Time limitations, however, prevented us from making the requisite suite of measurements needed to fully exploit that formalism. In addition to accumulating a more complete data sample, a successor experiment would also take advantage of the ability to broadcast, and study the reflections from, elliptically polarized signal of arbitrary ellipticity using the dual polarization ports of the Seavey horn antennas. Also particularly interesting would be data which might further reveal the frequency dependence of echo returns. Figure 16 displays the FFT, as a function of return time, for the 0° orientation (chosen at random). Although inconclusive, we observe considerable high-frequency power associated with, e.g., the return at ~ 10000 ns, consistent with expectations from density/COF scattering. A pure conducting plane reflector would be expected to be: a) uniform as a function of rotation in azimuth, and b) have a power spectrum falling inversely with frequency, at variance with our observations. With enough resolution, one might hope to observe the sequence of frequency-independent, frequency-dependent, and again frequency-independent returns (and over the full azimuth) that would be expected in a model where the scattering is dominated by density, acid, and COF effects, respectively. Additional data at higher power, and using a short-duration ‘tone’ would be very useful in this respect.

In the process of performing this measurement, one conspicuous pattern that emerges is the similarity of waveforms delineated by the optical axes we identify in this analysis. I.e., beyond 15000 ns, sharp scattering lines consistently appear at the same depth for data taken at angles $20^\circ - 90^\circ$; a different set of reflectors are evident for data taken at angles $-60^\circ - 10^\circ$ (and consistently within that angular interval). Similarly, signal shapes (sharp or extended) of internally reflected radio waves are repeatable within the two distinct angular ranges (Figs 17, 18, 19, 20); this is perhaps an indication that preferred crystal orientation is also accompanied by an asymmetry in absorption.

Finally, we re-emphasize that we have sensitivity only to the projection of the optical axis onto the vertical – the true birefringent asymmetry could, in principle, be much larger than the value reported here. The ARA experiment is expected to have the capability to broadcast in-ice signal horizontally over several km and should therefore provide essential vertical polarization information at radio frequencies.

Acknowledgments

The authors particularly thank Chris Allen (U. of Kansas) and Kenichi Matsuoka (U. of Washington) for very helpful discussions, as well as our colleagues on the RICE and ANITA experiments. We also thank Andy

Bricker of Lawrence High School (Lawrence, KS) for his assistance working with the Lawrence students. This work was supported by the National Science Foundation’s Office of Polar Programs (grant OPP-0826747) and QuarkNet programs. Any opinions, findings, and conclusions or recommendations expressed in this material are those of the author(s) and do not necessarily reflect the views of the National Science Foundation.

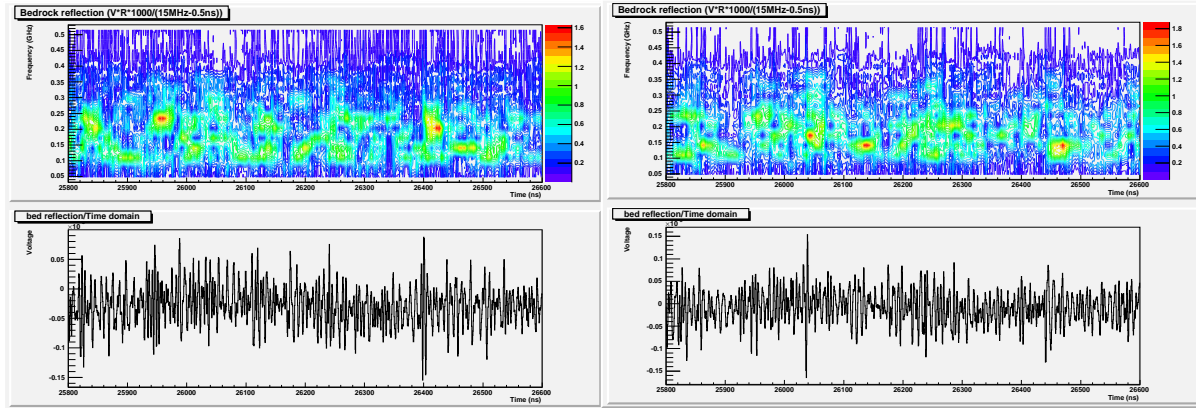


Figure 17: -10×0 Transmitter/Receiver orientation data, illustrating presence of possible return at 26.4 microseconds.

Figure 18: 30×30 Tx/Rx orientation; Although 26.4 microsecond return is absent, note presence of apparent return at 26.04 microseconds.

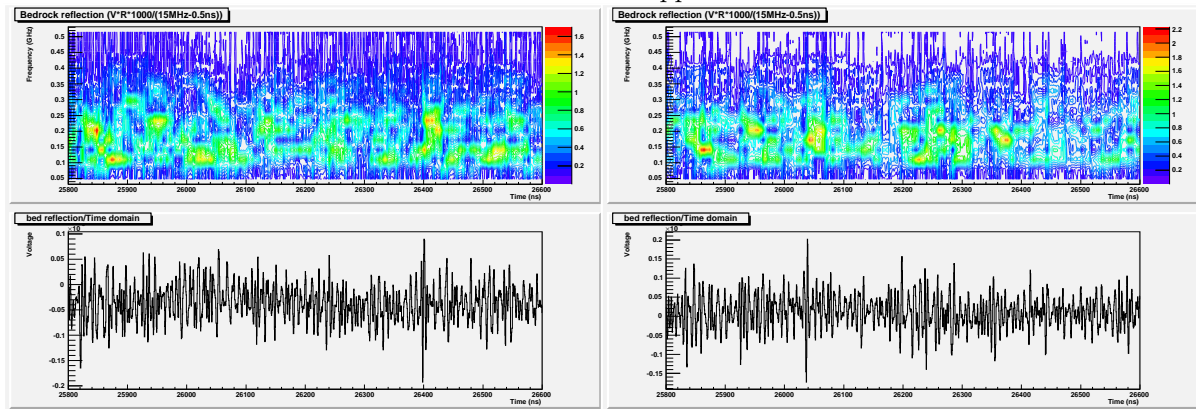


Figure 19: -30×-30 orientation data.

Figure 20: 50×60 orientation data.

References

Abassi, R. and 217 others, 2010. “IceCube Collaboration Contributions to the 2009 International Cosmic Ray Conference”, arXiv:1004.2093.

Kravchenko, I. and 20 others, 2006. “RICE limits on the diffuse ultrahigh energy neutrino flux”, *Phys. Rev. D* **73** (082002).

Gorham, P.W. and 40 others, 2009. “New Limits on the Ultrahigh Energy Cosmic Neutrino Flux from the ANITA Experiment”, *Phys. Rev. Lett.*, **103** (051103).

Gow, A., H. Ueda and D. Garfield, 1968. “Antarctic Ice Sheet: Preliminary Results of First Core Hole to Bedrock”, *Science*, **161**(3845), 1011.

ARA: The Askaryan Radio Array, approved by the National Science Foundation (April, 2010).

Ehringhaus, A, 1917. *Neus Jb. Miner Geol. Paläont*, **B41** (342-419).

- Auty, R. and R. Cole, 1952. "Dielectric Properties of Ice and Solid D_2O ." *J. Chem. Phys.* **20**(8), 1309.
- Hargreaves, N.D., 1977. "The polarization of radio signals in the radio echo sounding of ice sheets." *J. Phys. D, Appl. Phys.* **10**(9), 1285-1304.
- Hargreaves, N.D., 1978, "The radio frequency birefringence of polar ice." *J. Glac.* **21**, 301-313.
- Riffenburgh, B., 2008. *Encyclopedia of the Antarctic*.
- Siegert, M.J. and R. Kwok, 2000. "Ice-sheet radar layering and the development of preferred crystal orientation fabrics between Lake Vostok and Ridge B, central East Antarctica." *Earth and Planetary Science Letters*, **179**(2), 227-235.
- Price, P.B. and 9 others, 2002. Temperature profile for glacial ice at the South Pole: Implications for life in a nearby subglacial lake. *Proc. Nat. Acad. Sci.*, **99**(12), 7844-7877.
- CReSIS, 2008. <https://www.cresis.ku.edu/research/dataproductsandmodeling.html>
- Fujita, S., H. Maeno, and K. Matsuoka, 2006. "Radio-wave depolarization and scattering within ice sheets: a matrix-based model to link radar and ice-core measurements and its application", *J. Glac.*, **52**, 178.
- Matsuoka, K., T. Furukawa, S. Fujita, N. Maeno N, S. Uratsuka, R. Naruse, O. Watanabe, 2003. "Crystal orientation fabrics within the Antarctic ice sheet revealed by a multipolarization plane and dual-frequency radar survey." *J. Geophys. Res.* **108** (B10).
- Matsuoka, T., S. Fujita, S. Morishima and S. Mae, 1997. "Precise measurement of dielectric anisotropy in ice Ih at 39 GHz." *J. Appl. Phys.* **81**(5), 2344.
- Matsuoka, K., S. Uratsuka, S. Fujita, F. Nishio, 2004. "Ice-flow-induced scattering zone within the Antarctic ice sheet revealed by high-frequency airborne radar." *J. Glac.* **50**(170), 382-388.
- Besson, D.Z. and 42 others, 2008. "In situ radioglaciological measurements near Taylor Dome, Antarctica and implications for UHE neutrino astronomy." *Astropart. Phys.* **29**(2).
- Besson, D., R. Keast and R. Velasco, 2009. "In situ and laboratory studies of radiofrequency propagation through ice and implications for siting a large-scale Antarctic neutrino detector." *Astropart. Phys.*, **31**(5), 348-358.
- Doake, C., H. Corr, and A. Jenkins, 2002. "Polarization of radio waves transmitted through. Antarctic ice shelves." *Ann. Glac.* **34**(1), 165-170.
- Doake, C., H. Corr, A. Jenkins, K. Nichols, C. Stewart, 2003. "Applications of SAR Polarimetry and Polarimetric Interferometry." *Euro. Space Agency* **529**, 313-320.
- Fujita, S., T. Matsuoka, S. Morishima, S. Mae, 1993. "The measurement on the dielectric properties of ice at HF, VHF and microwave frequencies." *IEEE IGARSS '93*.
- Fujita, S. and S. Mae, 1993. "Relation between ice sheet internal radio-echo reflections at Mizuho Station, Antarctica." *Ann. Glac.* **17**, 269-75.
- Doake, C.S.M., 1981. "Polarization of Radio Waves Propagated through George VI Ice Shelf." *British Antarctic Survey Bulletin*.
- Woodruff, A.H. and C.S.M. Doake, 1979. "Depolarization of radio waves can distinguish between floating and grounded ice sheets." *J. Glac.* **23**, 223.
- Fujita, S., K. Matsuoka, H. Maeno, T. Furukawa, 2003. "Scattering of VHF radio waves from within an ice sheet containing the vertical-girdle-type ice fabric and anisotropic reflection boundaries." *Ann. Glac.* **37**, 305.
- Robin, G. de Q., Drewry, D. J., and Meldrum, D. T., 1977. "International studies of ice sheet and bedrock." *Philosophical Transactions of the Royal Society of London, Series B, Biological Sciences* 279(963), 185196.

- Fujita, S., Maeno, H., and Uratsuka, S., 1999, "Nature of radio echo layering in the Antarctic ice sheet detected by a two-frequency experiment." *Journal of Geophysical Research* 104, **B6**, 1301313024.
- Matsuoka, T., Fujita, S., Morishima, S., and Mae, S., 1997, "Precise measurement of dielectric anisotropy in ice Ih at 39 GHz" *Journal of Applied Physics*. 81(5), 2344-2348.
- Jiracek G. R., 1967. *University of Wisconsin Res. Rep. Ser. No. 67-1*
- Barwick, S., D. Besson, P. Gorham, D. Saltzberg, 2005. "South Polar *in situ* Radio Frequency Ice Attenuation." *J. Glac.* **04J067**
- Dowdeswell, J.A. and S. Evans, 2004. "Investigations of the form and flow of ice sheets and glaciers using radio-echo sounding." *Rep. Prog. Phys.*, **67**
- Kravchenko, I., D. Besson and J. Meyers, 2005. "*In situ* index of refraction measurements of the South Polar firn with the RICE detector", *J. Glac.* 03J061.
- Eisen, O., I. Hamann, S. Kipfstuhl, D. Steinhage, and F. Wilhelms, "Direct evidence for continuous radar reflector originating from changes in crystal-orientation fabric", *The Cryosphere*, 1, 2007, pp 1-10. <http://www.the-cryosphere.net/1/1/2007/>
- Eisen, O., F. Wilhelms, D. Steinhage and J. Schwander, 2006. "Improved method to determine RES-reflector depths from ice-core profiles of permittivity and conductivity", *J. Glac.* **52**, 177 (299-310)
- Martaan, C., G.H.Gudmandsson, H.Pritchard and O.Gagliardini, 2008. "Ice flow and crystal fabric near ice divides." *Geophys. Res. Abstracts*, **10**.

